

# Front lighting for an energy-harvesting luminous-reflective display and its design considerations

Tadamasa Anekawa, Mitsuhiro Shigeta, and Ichiro Fujieda \*

Ritsumeikan University, Department of Electrical and Electronic Engineering,  
Kusatsu, Japan

**Abstract.** The color gamut of a luminous-reflective display (LRD) shrinks when the incident light lacks blue photons. A frontlight unit (FLU) emitting in blue can prevent this and ensure readability in the dark. A one-dimensional model was developed to express spectral fluxes emerging from the subpixels in an energy-harvesting LRD (EH-LRD) in terms of its design parameters and the ambient lighting condition. In the experiment, a luminescent layer stacked on an infrared pass filter was excited by monochromatic light from an edge-lit FLU at 405 nm in the dark. The model roughly reproduced the relative peak intensities measured with the three materials (BBOT, Coumarin 6, and Lumogen F Red 305). It quantifies the trade-off between the two objectives of an EH-LRD: displaying images and harvesting energy. Hence, the model might be used to set goals for future developments of materials and components. © *The Authors*. Published by SPIE under a Creative Commons Attribution 4.0 International License. Distribution or reproduction of this work in whole or in part requires full attribution of the original publication, including its DOI. [DOI: [10.1117/1.OE.61.9.095102](https://doi.org/10.1117/1.OE.61.9.095102)]

**Keywords:** photoluminescence; reflective display; energy harvesting; frontlight; color gamut.

Paper 20220494G received May 10, 2022; accepted for publication Aug. 18, 2022; published online Sep. 5, 2022.

## 1 Introduction

The readability of emissive displays is poor under the sun.<sup>1</sup> A reflective display solves this problem by utilizing ambient light. Its contrast remains the same irrespective of illuminance. But its color gamut is narrow in general. Limiting the transmission bands of its color filters (CFs) can expand the color gamut only at the expense of luminance.<sup>2</sup> A practical design prioritizes luminance over color gamut. For example, the prototype reported in 2019 by one of the leading manufacturers has a color gamut covering only 19% of the triangle defined by the National Television System Committee (NTSC) in the Commission Internationale de l'Éclairage (CIE) 1931  $xy$  chromaticity diagram.<sup>3</sup> A luminous-reflective display (LRD) solves this dilemma by utilizing luminescent materials: its subpixel consists of an electro-optic shutter, a luminescent layer, a CF, and a reflector stacked in this order. Additive color mixing is accomplished by placing subpixels for three primary colors side by side.<sup>4,5</sup> Because the ambient light that is otherwise absorbed by CFs can be converted to photoluminescence (PL) photons, its luminance can exceed that of a conventional reflective display. Its color gamut is expected to be wider and more stable because the shapes of the PL spectra are independent of the excitation light. A spectral study on stacked structures of a luminescent layer, a CF, and a reflector confirmed these facts.<sup>6</sup> However, the color gamut of an LRD shrinks under the illumination lacking ultraviolet and blue photons. For example, as shown in figure 11 in Ref. 6, the color gamut measured under the illumination by a white light-emitting diode (LED) was 82% of the NTSC standard. It decreased to 44% when illuminated by a halogen lamp.<sup>6</sup> The luminescent materials used in this experiment were Coumarin 6 and Lumogen F Red 305 for the green and red subpixel, respectively, with no luminescent material for the blue subpixel. Using a blue-emitting backlight unit (BLU) and an appropriate dichroic filter has been proposed.<sup>7</sup> Because the ambient blue light passes through the dichroic filter as well, it cannot be utilized for displaying an image.

\*Address all correspondence to Ichiro Fujieda, [fujieda@se.ritsumei.ac.jp](mailto:fujieda@se.ritsumei.ac.jp)

By replacing the reflector with an infrared (IR) pass filter (IRpf) and a solar cell, one can harvest energy from the ambient light not utilized for displaying images.<sup>8</sup> This is one step forward from a mere energy-saving device. Such an energy-harvesting LRD (EH-LRD) might be applied for billboards and portable devices. Because ambient light is utilized for the two objectives, it is important to consider the trade-off between them. A model would link its design parameters and lighting conditions to the performance indices, such as luminance, color gamut, and photocurrent. The auxiliary light source for an EH-LRD must be a frontlight unit (FLU) rather than a BLU because its solar cell would block the blue light from such a BLU.

In this paper, a simple model for an EH-LRD is developed and checked by the experiment with an FLU. Using this model, utilization of ambient light for the two objectives is discussed.

## 2 One-Dimensional Model

A simple model relates input parameters (design parameters and ambient lighting condition) to performance indices (luminance, chromaticity coordinates, and photocurrent). As shown in Fig. 1, a luminescent layer (lum.), a CF, an IRpf, and a solar cell (PV) are stacked without a gap between each other. An electro-optic shutter (not shown) is placed above this structure to control the transmittance of ambient light. This constitutes a subpixel in an EH-LRD. We assume normal incidence for simplicity. Any angular dependencies of the material properties are neglected.

Let  $S_a$  be the spectral flux of the light incident on the luminescent layer, which absorbs  $S_a$  partially and emits PL photons. Let us denote this spectral flux as  $S_{PL}$ . Our goal is to express the upward spectral flux emerging from the top surface ( $S_{up}$ ), the downward spectral flux entering PV ( $S_{down}$ ) in terms of  $S_a$ , and the parameters characterizing each layer.

In the analysis below, the transmittance and reflectance of each layer are as defined in Fig. 1. They all depend on the wavelength  $\lambda$ . Here, we assume zero reflectance at each interface of lum., CF, and IR layers. This is justified because the refractive indices of these layers are similar, and we can eliminate the air gap at each interface. The transmittance of each layer is denoted as  $T_{LL}$ ,  $T_{CF}$ , and  $T_{IR}$ , respectively. Absorption is given by  $(1 - T_{LL})$ , etc. A solar cell has reflective electrodes on its top surface. Because its transmittance is zero, we use  $R_{PV}$  to denote its reflectance.

### 2.1 Spectral Fluxes

First, the spectral flux absorbed by the luminescent layer ( $S_{abs}$ ) is formulated. Three routes are considered. The first passage of  $S_a$  contributes  $(1 - T_{LL})S_a$ . The transmitted flux  $T_{LL}S_a$  can be absorbed via two ways: the second passage after the reflection by IRpf contributes  $(1 - T_{LL})(1 - T_{IR})T_{CF}^2T_{LL}S_a$  and the reflection by PV adds  $(1 - T_{LL})R_{PV}T_{IR}^2T_{CF}^2T_{LL}S_a$ . Hence,  $S_{abs}$  is given as

$$S_{abs} = (1 - T_{LL})[1 + (1 - T_{IR} + R_{PV}T_{IR}^2)T_{CF}^2T_{LL}]S_a. \tag{1}$$

Second, let us express the spectrum of the PL photons generated by the luminescent material. Denoting the quantum yield of the luminescent material as  $\eta_{QY}$ , the total number of PL photons generated is given as  $\eta_{QY} \int S_{abs}(\lambda) d\lambda$ . These are distributed over a certain wavelength range, and

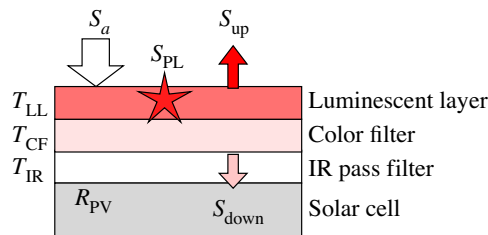


**Fig. 1** Cross section of the layered structure that constitutes the subpixel in an EH-LRD. An electro-optic shutter above the luminescent layer (not shown) controls the transmittance of the incident light.

this distribution is denoted  $S_{em}$ . Assuming that  $S_{em}$  is normalized ( $\int S_{em}(\lambda)d\lambda = 1$ ), the spectrum of the PL photons inside this structure  $S_{PL}$  is given as

$$S_{PL}(\lambda) = \eta_{QY} S_{em}(\lambda) \int S_{abs}(\lambda)d\lambda. \quad (2)$$

Third, we consider the upward and downward spectral fluxes exiting the luminescent layer. The upward flux  $S_{up}$  is formulated as follows. The PL photons contribute via three routes. One half of  $S_{PL}$  goes upward directly. The other half goes downward. It is partially reflected by either IRpf or PV. Multiplying  $S_{PL}(\lambda)/2$  by the corresponding probabilities gives the upward flux inside this wave-guiding structure. Note that  $S_{PL}$  is the spectral flux inside this structure. For the outgoing upward flux, the probability of light extraction  $\eta_{ext}$  needs to be multiplied. In addition, the flux  $S_a$  passing through the luminescent layer can go upward after being reflected by either IRpf or PV. Multiplying  $T_{LL}S_a$  by the corresponding probabilities gives this contribution from the ambient light. Hence, the upward flux exiting the luminescent layer is expressed as

$$S_{up} = \eta_{ext} \left\{ 1 + (1 - T_{IR} + R_{PV}T_{IR}^2)T_{CF}^2T_{LL} \right\} \frac{S_{PL}}{2} + (1 - T_{IR} + R_{PV}T_{IR}^2)T_{CF}^2T_{LL}^2S_a. \quad (3)$$

The expression for the downward spectral flux  $S_{down}$  is derived in a similar manner. There are two components. The first is the downward PL photons passing CF and IRpf and avoiding reflection by PV. The second is the incident light passing all of the layers and avoiding reflection at the PV surface. Hence, the downward flux is given as

$$S_{down} = T_{CF}T_{IR}(1 - R_{PV}) \left( \frac{S_{PL}}{2} + T_{LL}S_a \right). \quad (4)$$

Tristimulus values are calculated from the spectral flux  $S_{up}$  and the CIE color matching functions. A color gamut is defined by these chromaticity coordinates. It specifies how vivid a displayed image can be.

One can prioritize energy harvesting by eliminating IRpf in Fig. 1. For such a configuration, the spectral fluxes are calculated by setting  $T_{IR}$  to unity in Eqs. (3) and (4).

## 2.2 Numerical Example

Luminescent solar concentrators (LSCs) utilize luminescent materials to generate power by converting ambient light to PL photons.<sup>9</sup> Simple down-conversion is also applied for improving spectral matching to solar cells.<sup>10</sup> A wide variety of luminescent materials exists, and the quest for ideal materials continues in these fields.

In this numerical example, we select BBOT, Coumarin 6, and Lumogen F Red 305 for each primary color because they are readily available for proof-of-concept experiments. In fact, we fabricated luminescent layers with these materials.<sup>8</sup> The emission spectra and the spectral transmittances measured with some off-the-shelf CFs are reproduced in Figs. 2(a) and 2(c), respectively. The data in Fig. 2(b) are obtained by scaling the absorption coefficients in the literature<sup>11,12</sup> based on the transmittances of these layers measured at 450 nm.<sup>8</sup> We purchased an IRpf and measured its spectral transmittance. The reflectance and the external quantum efficiency of a commercial polycrystalline solar cell were also measured. These results are shown in Fig. 2(d) together with the CIE luminous efficiency function.

It is well known that a planar waveguide traps PL photons by total internal reflection. This is the operation principle of an LSC. The probability of trapping PL photons in a wave-guiding structure is well studied for this application.<sup>13</sup> For an LRD, the PL photons need to be extracted as much as possible. A diffuse reflector increases the probability of light extraction.<sup>6,8</sup> In this numerical example, we set  $\eta_{ext}$  in Eq. (3) to unity for simplicity and neglect its dependency on the wavelength.

As for the input parameter  $S_a$ , the standard solar spectrum air mass 1.5 global (AM 1.5G)<sup>14</sup> is selected. This is shown by the dotted curve in Fig. 3. The unit of its ordinate is proportional to the

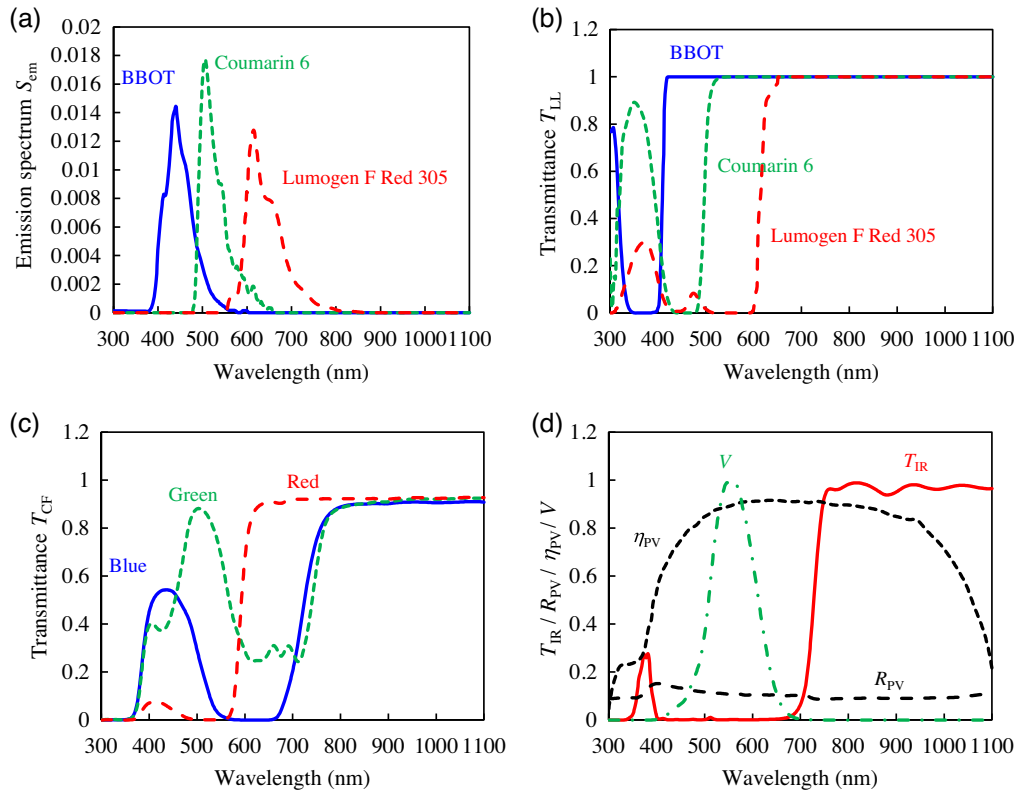


**Fig. 2** Input parameters for the model. (a) Emission spectra of the three luminescent materials. (b) Transmittance of the luminescent layers. (c) Transmittance of the CFs. (d) Transmittance of the IRpf, reflectance, and external quantum efficiency of the solar cell and the CIE luminous efficiency function.

number of photons rather than Watt (W). The spectrum is normalized such that  $\int S_a(\lambda) d\lambda = 1$ . Note that there are a lot of IR photons in this spectrum.

Plugging the parameters in Fig. 2 and the AM 1.5G spectrum into the equations above generates the spectral fluxes for the two objectives. Each colored curve in Fig. 3 represents the upward flux from the simulated subpixel for each primary color. The downward fluxes are shown in Fig. 4 in a similar manner. The fluxes from the two configurations with and without IRpf are compared in both figures. The layered structure is as indicated in each graph. The AM 1.5G spectrum serves as a reference.

The fluxes in Fig. 3(a) are larger than those in Fig. 3(b) roughly by a factor of 2. This is because IRpf reflects the downward fluxes in the visible range. The blue curves in Fig. 3 are

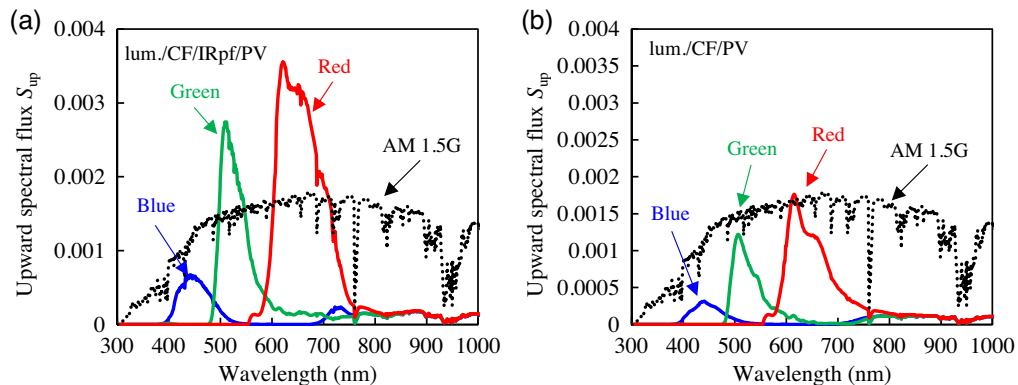


**Fig. 3** Spectral fluxes to be utilized for displaying images for each configuration: (a) with and (b) without the IRpf.

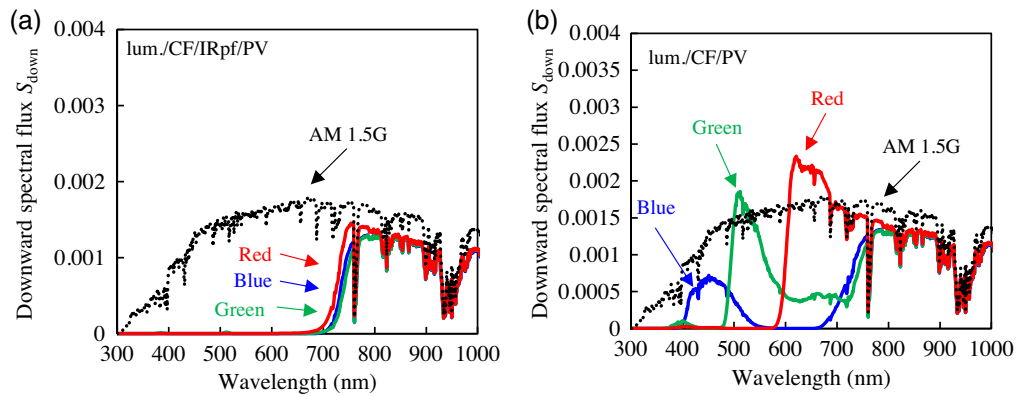


**Fig. 4** Spectral fluxes to be utilized for harvesting energy for each configuration: (a) with and (b) without the IRpf.

relatively small. This does not pose a problem for displaying white because we can always monitor the ambient light and adjust the transmittance of each electro-optic shutter accordingly.

In Fig. 4(a), there are no downward fluxes in the visible range, and the three curves are almost identical. This configuration prioritizes energy harvesting. The red curve around 750 nm is slightly larger. This wavelength range is where the IRpf transmittance ( $T_{IR}$ ) abruptly varies, as shown in Fig. 2(d). In Fig. 4(b), the shapes of the spectra in the visible range resembles those in Fig. 3(a). They have the same two components: the PL photons and the transmitted incident light.

In Fig. 3(a), the upward fluxes in the red and green wavelength ranges exceed the incident flux. This is the very reason that an LRD can be brighter than a purely reflective display: the effect of downconversion by the luminescent materials.<sup>5-8</sup> Among the three subpixel configurations, the red one always has the largest spectral flux, and the green one follows. This is related to the wavelength range that these materials can utilize. A red-emitting material converts blue and green incident light, whereas a blue-emitting material utilizes ultraviolet light only. In Fig. 3(b), the upward flux exceeds that of the incident light only around 600 nm. The configuration without IRpf sacrifices the advantage in luminance and prioritizes energy harvesting.

In addition, chromaticity coordinates for the two-layered configurations are shown in Fig. 5. The color gamut is comparable to the NTSC standard. As shown by the open squares, insertion of IRpf extends it slightly. The light reflected by IRpf needs to pass the two layers (CF and lum.), and this extra distance narrows the spectra, as shown in Figs. 3(a) and 3(b).

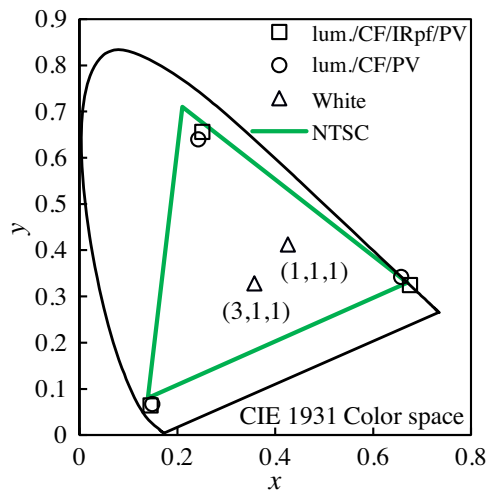


**Fig. 5** Chromaticity coordinates calculated for the configurations with and without IRpf (square and circle markers, respectively). The open triangles are those for a white point. The numbers in the parenthesis are the weighting factors for the spectrum addition.

The open triangles in Fig. 5 are the coordinates of a white point for the configuration with IRpf. They are calculated by adding the spectra in Fig. 3. The three numbers indicate the weighting factors for this addition. In practice, we can set these factors by controlling the transmittance of each electro-optic shutter. Because the blue curves in Fig. 3 are relatively small, equal weighting (1, 1, 1) results in the white point (0.43, 0.41). When the weighting factor for the blue spectrum is set to 3, it moves to (0.36, 0.33). Note that these results are based on the characteristics of the materials at hand. There are opportunities to improve  $T_{CF}$  in Fig. 2(c) for example.

### 3 Experiment

In complete darkness, an auxiliary light source is required for a reflective display. For an LRD, an FLU emitting blue light will increase the luminance of all three colors. In this section, we describe the experiment with such an FLU and some layered structures. The input parameters for the model in Sec. 2 are drastically simplified by adopting a monochromatic light source and eliminating the CFs. Hence, this experiment serves as a test for the model.

#### 3.1 Frontlight Unit

In a commercial e-book reader (Amazon Kindle, Model J9G29R), an edge-lit FLU illuminates an electrophoretic display. In this FLU, four white LEDs are installed at the edge of a light-guide plate. Some microstructures are distributed on its surface to extract the light toward the reflective display. Their density is set higher at the region further away from the LEDs. In this way, the loss of light propagating inside is compensated for, leading to uniform illumination.

We removed the white LEDs and attached a light-diffusing film (Tsujiiden Co., Ltd., Model D114) on the edge surface of the plate. As shown in Fig. 6(a), a laser module is positioned such that its beam enters the film normally. A black acrylic plate was placed at the edge to block any light leakage from the light source side. A black cloth was placed beneath the FLU to absorb the light extracted downward. A photograph of this setup is shown in Fig. 6(b). When the laser is turned on in the dark, the scattered light spreads inside the light-guide plate. Unfortunately, as shown in Fig. 6(c), the blue light leaks toward an observer. Nevertheless, this leakage degrades

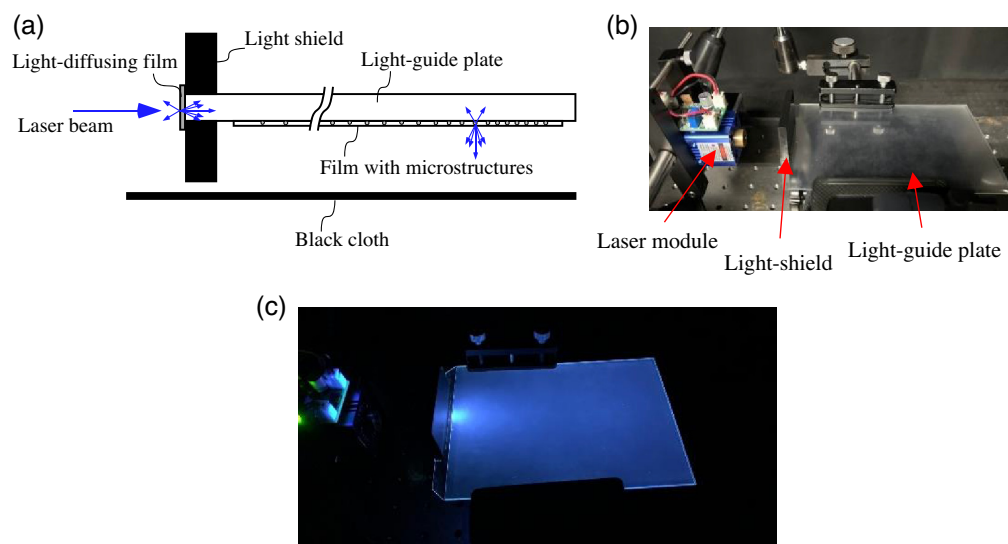


**Fig. 6** A schematic drawing and photographs of the experimental setup. (a) Cross section of the modified FLU. A laser module is placed near the light-guide plate. (b) Photograph of the setup. (c) The laser light (wavelength 405 nm) hits the film and the scattered light spreads inside the light-guide plate. The microstructures at the surface of the plate extract them. A black cloth placed beneath the FLU absorbs the downward light, and the upward light from the FLU is recorded in this picture.

the contrast ratio of the images to be displayed. The light extracted downward is larger as will become clear later.

In this experiment, three luminescent materials were used for the three primary colors: BBOT, Coumarin 6, and Lumogen F Red 305. A thin layer of each material was formed on a 50 mm × 50 mm × 1.0 mm acrylic plate. Its preparation procedure is described elsewhere.<sup>8</sup> The emission spectra from these layers are shown in Fig. 2(a). A 25 mm × 25 mm × 3.2 mm IRpf was attached to its bottom surface. As shown by the curve marked as  $T_{\text{IR}}$  in Fig. 2(d), the transmittance of this filter drops abruptly at about 700 nm. Note that this is for the case of normal incidence. We purchased an adhesive film developed for attaching a polarizer film to the surface of a liquid-crystal display (LCD) panel. This film was used to eliminate the air gap between the acrylic plate and IRpf.

As shown in Fig. 7(a), each layered structure was placed beneath the modified FLU. The downward blue light from the FLU illuminated each luminescent layer, denoted as “lum.” in Fig. 7(a). Images captured by a camera are shown in Figs. 7(b)–7(d). In addition to the upward PL photons from the luminescent layers, any light leaking from the FLU upward is recorded in these pictures. Emission from each lum. area appears uniform, indicating that illumination by the FLU is uniform over this area. The central 25 mm × 25 mm region is covered by IRpf, and it appears brighter than the surrounding 50 mm × 50 mm area. In this region, the downward PL flux from the luminescent layer and the unabsorbed excitation light from the FLU are added after being reflected by IRpf. Note that the edge surface of the acrylic plate appears brighter. Some PL photons are trapped in the light-guide plate. They propagate inside, become concentrated, and escape from the edge surfaces.

### 3.2 Measurement

Spectrum measurement allows us to distinguish the PL photons from the luminescent layer and any background light leaking from the FLU. As shown in Fig. 8(a), an optical fiber head is held

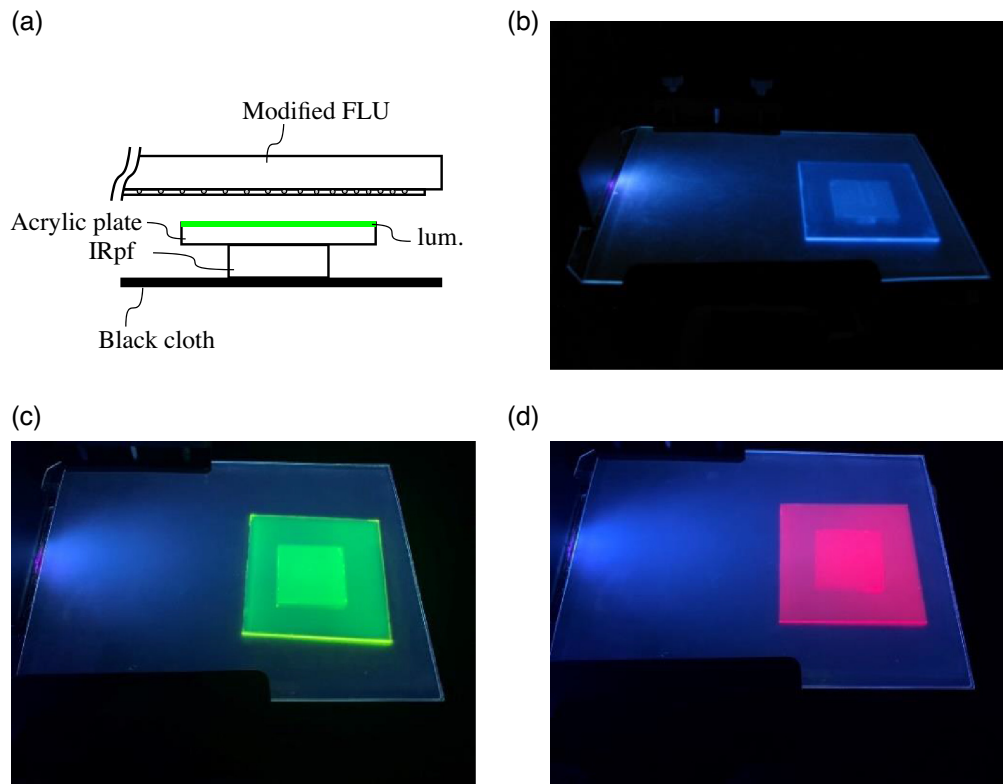


**Fig. 7** Excitation of the luminescent layers by the modified FLU. (a) Cross section of the experimental setup. The luminescent materials are (b) BBOT, (c) Coumarin 6, and (d) Lumogen F Red 305.

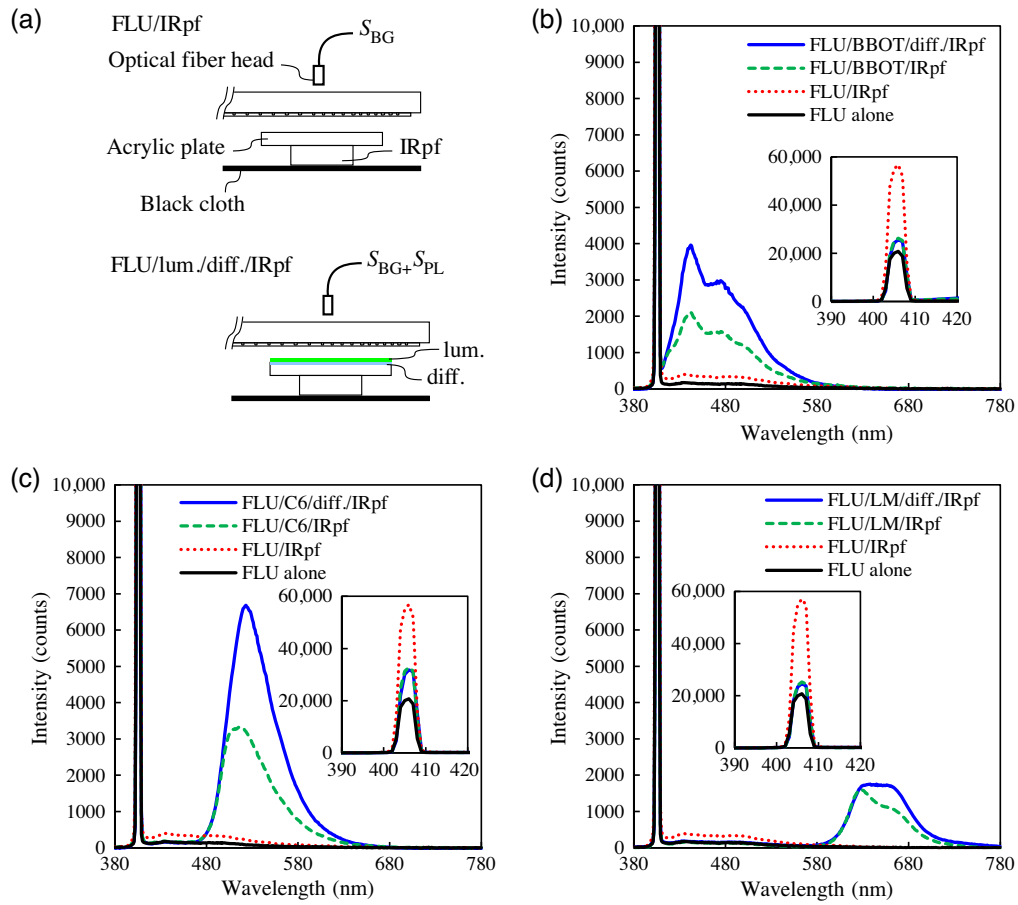


**Fig. 8** Spectrum measurement for identifying the PL photons from a luminescent layer. (a) Setup for the measurement with and without a luminescent layer. The luminescent materials used for measuring the spectra in panels (a)–(d) are (b) BBOT, (c) Coumarin 6, and (d) Lumogen F Red 305. Each inset shows magnified spectra around 405 nm.

in the vicinity of the FLU, above the center of IRpf. It guides the light from the fixed region of the FLU to a spectrometer. First, only the acrylic plate attached to IRpf is illuminated by the FLU. The spectrum acquired in this case (Flu/IRpf) is denoted as  $S_{BG}$ . When a luminescent layer is present, the PL photons from it can reach the spectrometer. The spectrum recorded in this case is expressed as  $\eta_{ext}S_{PL} + S_{BG}$ , where  $\eta_{ext}$  is the light extraction efficiency and  $S_{PL}$  is the spectrum of the PL photons generated inside the luminescent layer. The component  $\eta_{ext}S_{PL}$  is obtained from these two measured spectra. For the configuration FLU/lum./diff./IRpf, a light-diffusing film (diff.) is inserted to extract the PL photons trapped inside this light-guiding structure. The air gap between each layer is eliminated by the adhesive film described earlier. The spectrum recorded with the configuration without the light-diffusing film (FLU/lum./IRpf) shows the effect of the film on  $\eta_{ext}$ . The measured spectra are compared in Figs. 8(b)–8(d) for each luminescent material. The legends specify the layered structures. Each inset shows magnified spectra around 405 nm.

The black curve labeled as “FLU alone” is the spectrum recorded with the FLU placed above the black cloth. Because the downward light is absorbed, only the light emitted upward by the FLU is recorded. This curve represents the background to be subtracted from the spectra acquired with a luminescent layer. Unexpectedly, low-intensity emission is observed up to about 580 nm. The relative magnitude of this component remains the same irrespective of the distance between the measurement spot and the edge of the light-guide plate. Hence, it is likely that some luminescent materials are contained in the film with the microstructures.

The dotted red curve labeled as “FLU/IRpf” is the spectrum acquired with the configuration Flu/IRpf. The downward light reflected by IRpf is added to the upward light. The intensity at

405 nm is more than doubled, as shown in the inset. Ideally, the peak intensity ratio for the red and black curves should be infinity if no light leaks upward from an FLU. We discuss this issue in Sec. 4.3.

As shown by the solid blue and broken green curves in Figs. 8(b)–8(d), PL photons are observed in the wavelength range intended for each color. The light-diffusing film increases these intensities, especially for the green and blue luminescent materials. Specifically, scattering enhances the light extraction efficiency more at shorter wavelengths.

A closer look at each peak by the PL photons in Fig. 8 reveals that there is little change at shorter wavelengths. Self-absorption in the luminescent layers hinders the emission at shorter wavelengths.<sup>9,15</sup> One might expect that the absorbed energy is liberated in the form of PL photons. However, the measured intensity of the re-emitted PL photons from a planar waveguide is at least four orders of magnitude smaller than the original emission.<sup>16</sup> It is likely that the phenomenon of self-absorption in the luminescent layer masks the potential gain brought by the light-diffusing film in the shorter wavelength range for each color.

The insets in Fig. 8 indicate that the downward excitation light is mostly absorbed by the luminescent materials. It also shows that it is partially reflected by IRpf. As is shown next, the color gamut calculated from these spectra becomes narrower by this component. This is because there are no CFs under the luminescent layers to absorb the transmitted excitation light in this experiment.

### 3.3 Analysis

The result of the background subtraction is shown in Fig. 9(a) for each luminescent material. The solid curves are for the structures with the light-diffusing film, and the dotted curves are for those without it. The light-diffusing film increases the peak intensities by a factor of two for the blue and green material, whereas this gain is not much for the red material. This behavior might be attributed to the change in the probability  $\eta_{\text{ext}}$ . Because the blue and green PL photons are scattered in wider angular ranges than the red photons, they are more likely to be extracted from the layered structures.

The CIE 1931 color matching functions are used to calculate chromaticity coordinates in Fig. 9(b). The square and triangle markers are the coordinates from the six curves in Fig. 9(a). The open circles are those from the measured spectra in Fig. 8 (FLU/lum./IRpf). Compared to the NTSC standard, the areas of these triangles increase from 39.7% (circle markers) to 73.1% (square markers) and 74.6% (triangle markers). The light-diffusing film slightly extends the color gamut. For the red material, this trend is reversed. This is due to the broadening of the

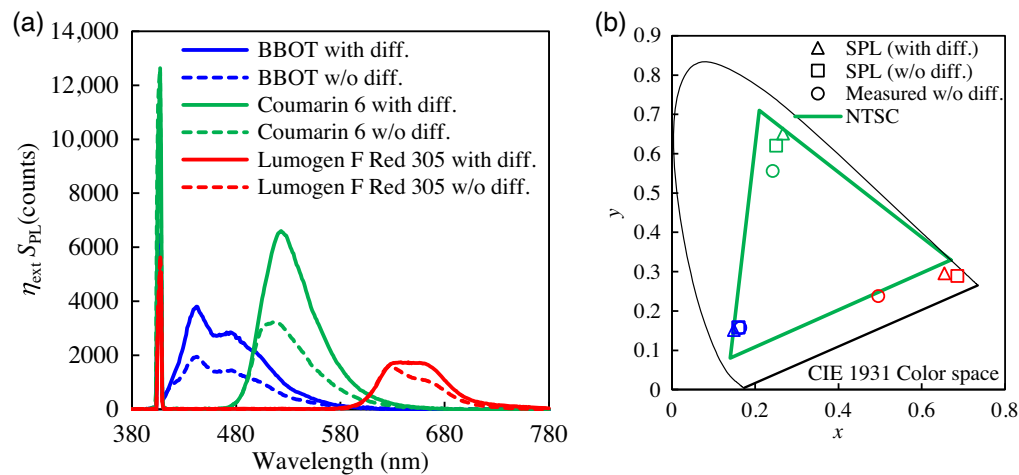


**Fig. 9** The PL components exiting the luminescent layers. (a) Spectra measured with the luminescent layers after subtracting the background component from the FLU. (b) Chromaticity coordinates calculated from the spectra in panel (a) (square and triangle markers). Open circles are from the spectra measured without the light-diffusing film (FLU/lum./IRpf in Fig. 8).

spectrum, as shown in by the red solid curve in Fig. 9(a). The color gamut can be further expanded by inserting CFs between the luminescent layers and IRpf. Nevertheless, this is accomplished at the expense of luminance.

## 4 Discussions

### 4.1 Model and Experiment

For checking the validity of the model, let us assume a monochromatic incident light at 405 nm, no absorption by the CFs, and perfect reflection by the reflector. Specifically, the input parameters for the model assumed in Sec. 2 are modified as follows:  $S_a = \delta(405)$ ,  $T_{CF} = 1$ , and  $T_{IR} = 0$ . For the moment, the probability of light extraction  $\eta_{ext}$  in Eq. (3) is assumed to be unity, i.e., no trapping of PL photons in the layered structures. The upward spectral fluxes calculated by the model under these assumptions are shown by the solid curves in Fig. 10.

In Fig. 10(a), the spectra measured without the diffuser film are reproduced for comparison. The scale for the second y-axis is adjusted such that the measured peak intensity for the green material approximately matches the model. The relative peak intensities are about the same for all three materials. The peak wavelengths are slightly shifted toward longer wavelengths. This redshift is likely to be caused by the self-absorption inside luminescent layers. Specifically, the PL photons propagate longer distances inside the layer after being scattered, and those with shorter wavelengths are absorbed by its own material. In fact, the PL spectrum from a uniform luminescent layer depends on its emission angle because of self-absorption in the layer.<sup>15</sup> The current model cannot handle oblique propagation.

Next, the spectra measured with the diffuser film is compared with the model calculation in Fig. 10(b). The redshift in each measured spectrum becomes larger. After being scattered by the diffuser film, the PL photons need to traverse longer distances in the luminescent layer. Hence, they suffer more from self-absorption. This results in a larger redshift. In addition, the spectrum measured with the red material is quite deformed. This might be explained by considering the change in the cut-off wavelength of an interference filter. As shown in Fig. 2(d), the IRpf used in the experiment reflects the light below 700 nm. This is valid for normal incidence. When the red light enters the filter obliquely, they are more likely to be transmitted. Hence, the model overestimates the spectral intensity for this subpixel at wavelengths shorter than 700 nm.

Another discrepancy from the experiment is notable at the wavelengths <405 nm in Fig. 10. When the monochromatic light at 405 nm is absorbed in the experiment, no PL photons are generated below 405 nm. The law of energy conservation prohibits emission below the excitation wavelength. This fact is not implemented in the model.

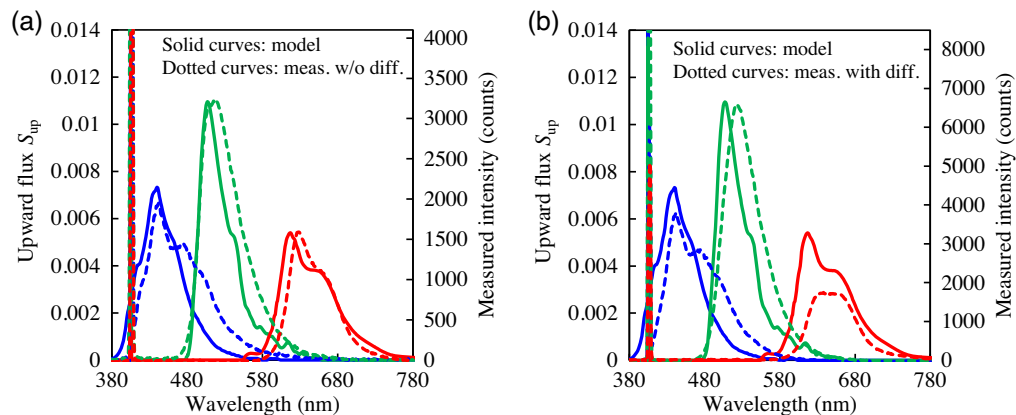


**Fig. 10** Comparison of the model and the experiment. Solid curves are the spectra calculated for the layered structure lum./IRpf. The model assumes monochromatic excitation at 405 nm, no CFs, 100% reflection by the reflector, and 100% extraction of PL photons. Dotted curves are reproduced from Fig. 9(a). Those in panel (a) are the spectra measured without the diffuser film. Those in panel (b) are the spectra measured with the diffuser film.

## 4.2 Ambient Light Utilization

Although the current model does not provide exact answers, it helps us understand which design parameters are important for better performance. In this section, we discuss the trade-off between energy-harvesting and displaying images. With the design parameters in Sec. 2, we show how far apart the current level of performance is from an ideal case.

Let us define performance indices appropriate for an EH-LRD. Luminance and photocurrent come to mind immediately. They are measurable with standard instruments. Here, we define two indices as follows:

$$\varepsilon_L = \int V(\lambda)S_{\text{up}}(\lambda)d\lambda / \int S_a(\lambda)d\lambda, \quad (5)$$

$$\varepsilon_{\text{ph}} = \int \eta_{\text{PV}}(\lambda)S_{\text{down}}(\lambda)d\lambda / \int S_a(\lambda)d\lambda, \quad (6)$$

where  $V$  and  $\eta_{\text{PV}}$  are the CIE luminous efficiency function and the external quantum efficiency of a solar cell, respectively. These dimensionless quantities imply the efficiency of converting the input to something of value. The index  $\varepsilon_L$  becomes maximum if  $S_{\text{up}}$  is equal to  $S_a$ . This corresponds to the case of a perfect reflector. The index  $\varepsilon_{\text{ph}}$  peaks when  $S_{\text{down}}$  is set to  $S_a$ . This is equivalent to the case of a bare solar cell.

Next, the two performance indices were calculated from the spectral fluxes in Figs. 3 and 4 and the efficiency curves in Fig. 2(d). The open markers in Fig. 11 represent the indices for the structures with IRpf and the solid markers for those without it. The circle, square, and triangle markers correspond to the indices for the luminescent materials BBOT, Coumarin 6, and Lumogen Red F 305, respectively. The vertical dotted line and the horizontal broken line indicate the upper limits for the two indices.

The index  $\varepsilon_{\text{ph}}$  is almost the same for the three subpixel configurations with IRpf (open markers). When IRpf is removed,  $\varepsilon_{\text{ph}}$  increases at the expense of  $\varepsilon_L$  (solid markers). The incident energy is directed either up or down. One cannot have large indices simultaneously. The horizontal broken line and the vertical dotted line indicate the upper limits of the two efficiencies:  $\varepsilon_L = 0.176$  for a perfect reflector and  $\varepsilon_{\text{ph}} = 0.804$  for a bare solar cell. The major loss mechanisms are the absorption by the CFs and nonunity  $\eta_{\text{PV}}$ . An LRD needs CFs to absorb the

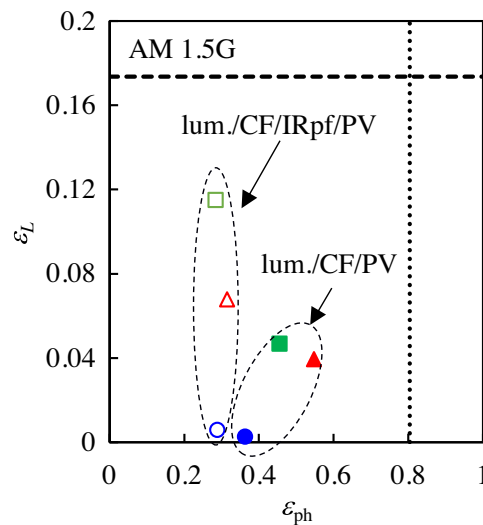


**Fig. 11** The trade-off between the two objectives is expressed by the two performance indices: light utilization efficiency for displaying images and harvesting energy. The horizontal broken line and the vertical dotted line indicate the upper limit for each index corresponding to a perfect reflector and a bare solar cell, respectively.

excitation light passing through the luminescent materials. Therefore, absorption by CFs is inevitable, and the upper limits will never be achieved.

The index  $\varepsilon_L$  for the blue subpixel is significantly smaller than those for the other two colors. This is partly because  $V$  is smaller and partly because there are not many photons in the AM 1.5G spectrum to excite BBOT. An auxiliary light source may be used as described in Sec. 3. Alternatively, one can enlarge the blue subpixel area to compensate for the low luminance. A new material would help.

### 4.3 Future Development

Light leakage from an edge-lit FLU toward an observer degrades the contrast ratio and the color gamut. In this respect, the organic LED (OLED) technology is well suited for enhancing readability of a reflective display in general. Emission from an OLED with a reflective electrode is usually one-sided. Apertures can be fabricated in an OLED to let ambient light go through. Other advantages of the OLED technology include compactness and uniform illumination over a large area. This concept was conceived two decades ago,<sup>17</sup> and it was demonstrated independently with a reflective LCD.<sup>18</sup> The OLED technology is certainly useful for an LRD. An FLU would block some of the incoming light, and it would consume some power. Discussion on this trade-off for adding an FLU requires quantitative analysis for each specific application. Practical design considerations such as this deserve attention in future.

The LCD technology is a good candidate for the optical shutter in an LRD. A commercial LCD panel, including its CFs and polarizers, is highly transparent in the near-IR wavelength range.<sup>19</sup> Monocrystalline and polycrystalline silicon solar cells have high power conversion efficiency in this wavelength range. Compactness is required for mobile applications. A 0.2-mm-thick LCD panel has been demonstrated.<sup>20</sup> Thin glass substrates have been developed for flexible OLED applications.<sup>21</sup> This knowledge might encourage one to stack an FLU, a thin LCD panel without CFs, an array of luminescent layers, CFs, and IRpfs on a Si-based solar cell. Alternatively, integration of components will simplify the device structure of an LRD. For example, in-cell polarizer technology<sup>22</sup> will be useful for an LRD. It might be worthwhile to consider integrating an OLED-based FLU in an electro-optic shutter. As these technologies mature and various materials become available, the OLED-LCD integration proposed in the past<sup>23,24</sup> might be considered for an LRD in the future.

Regarding luminescent materials, we used organic dyes in our experiment to check the validity of the model. They are widely available, and their properties are well documented. By contrast, quantum dots and quantum rods have been intensively studied for applications such as LCDs,<sup>25</sup> micro-LED displays,<sup>26</sup> and LSCs.<sup>27</sup> Their narrow emission spectra result in a larger color gamut for display applications. Large Stoke's shift mitigates the photon loss due to self-absorption in LSCs. These advantages of quantum dots and rods are expected for EH-LRDs as well.

## 5 Conclusions

An LRD is expected to be brighter than a purely reflective display because some of the ambient light otherwise absorbed by CFs are converted to PL photons. Its color gamut can be wider and more stable because the shapes of the PL spectra are independent of the excitation light. Under the illumination lacking ultraviolet and blue photons, however, blue-emitting material might not be excited. Then, blue subpixel needs to rely on reflection only, leading to a narrower color gamut. An auxiliary light source will prevent this and ensure readability in the dark as well. For an EH-LRD, it must be an FLU because its solar cell would block the light from a BLU. A one-dimensional model has been developed for an EH-LRD. The spectral fluxes from its subpixels are expressed in terms of its design parameters and ambient lighting condition. Luminance, chromaticity coordinates, and photocurrent are calculated from them. In an experiment, the FLU in an Amazon Kindle was modified to emit monochromatic light at 405 nm. It illuminated a luminescent layer stacked on an IRpf. The model roughly reproduced the relative peak intensities measured with three materials (BBOT, Coumarin 6, and Lumogen F Red 305).

The measured spectra were slightly redshifted. This is because the PL photons propagating obliquely in the luminescent layers suffer more from self-absorption. The current one-dimensional model cannot handle oblique propagation. Insertion of a light-diffusing film between the luminescent layer and the IRpf doubled the spectral intensities for the blue and green materials, indicating that more PL photons are extracted from the layered structures. The spectrum measured with the red material was deformed. This is attributed to the angle-dependent transmittance of the IRpf. Light leakage from an edge-lit FLU toward an observer degraded the contrast ratio and the color gamut in this experiment. The spectral measurements allowed us to remove this component, and the color gamut covered about 74% of the NTSC standard in the CIE 1931  $xy$  chromaticity diagram. An FLU based on the OLED technology is a solution to this problem because its emission can be completely one-sided. Nevertheless, inserting CFs would expand the color gamut further at the expense of luminance. An EH-LRD utilizes ambient light for the two objectives: displaying images and harvesting energy. The model quantifies the trade-off between them. It shows how far apart the calculated characteristics are from an ideal case. Thus, it might be used to set goals for future developments of materials and components. An EH-LRD will add flexibility to the power management system of billboards and portable displays.

## Acknowledgments

We would like to thank Shiori Matsuda and Yu Kawano for the measurement of the spectral transmittances of the optical films and the quantum efficiency of the solar cell described in Sec. 2. Our gratitude is extended to Yuki Kanai, Hiroto Nishimura, and Yuta Mizuno for assisting with the experiment described in Sec. 3. The authors declare no conflicts of interest.

## Code, Data, and Materials Availability

We are happy to provide digital data upon request.

## References

1. H.-W. Chen et al., "Liquid crystal display and organic light-emitting diode display: present status and future perspectives," *Light Sci. Appl.* **7**, 17168 (2018).
2. C.-K. Liu, T.-H. Yang, and K.-T. Cheng, "Expanding color gamut of reflective liquid crystal displays from filtering undesirable wavelengths of a light source by an embedded etalon," *Appl. Opt.* **56**(7), 1880–1885 (2017).
3. H. Hakoi et al., "High-performance and low-power full color reflective LCD for new applications," in *SID Symp. Dig. Tech. Pap.*, Vol. 50, pp. 279–282 (2019).
4. O. Okumura, Patent application JP-A-2001-264756 (in Japanese).
5. G. A. Gibson et al., "Luminescent enhancement of reflective displays," in *23rd Annu. Meet. of the IEEE Photonics Soc.*, Denver, CO, pp. 69–70 (2010).
6. I. Fujieda, Y. Tsutsumi, and S. Matsuda, "Spectral study on utilizing ambient light with luminescent materials for display applications," *Opt. Express* **29**(5), 6691–6702 (2021).
7. G. Gibson et al., "Fast full-color reflective display via photoluminescent enhancement," *J. Soc. Inf. Disp.* **20**(10), 552–558 (2012).
8. S. Matsuda et al., "Luminance, color gamut, and energy-harvesting characteristics of luminescent layers placed above a solar cell," *Opt. Express* **29**(22), 36784–36795 (2021).
9. I. Papakonstantinou, M. Portnoi, and M. G. Debije, "The hidden potential of luminescent solar concentrators," *Adv. Energy Mater.* **11**, 2002883 (2021).
10. E. Klampaftis et al., "Enhancing the performance of solar cells via luminescent downshifting of the incident spectrum: a review," *Sol. Energy Mater. Sol. Cells* **93**, 1182–1194 (2009).
11. J.-K. Kim, S.-H. Joo, and J.-K. Song, "Reflective-emissive photoluminescent cholesteric liquid crystal display," *Appl. Opt.* **52**(34), 8280–8286 (2013).

12. L. R. Wilson and B. S. Richards, "Measurement method for photoluminescent quantum yields of fluorescent organic dyes in polymethyl methacrylate for luminescent solar concentrators," *Appl. Opt.* **48**(2), 212–220 (2009).
13. C. L. Mulder et al., "Dye alignment in luminescent solar concentrators: I. Vertical alignment for improved waveguide coupling," *Opt. Express* **18**, A79–A90 (2010).
14. G. P. Smestad et al., "Reporting solar cell efficiencies in solar energy materials and solar cells," *Sol. Energy Mater. Sol. Cells* **92**(4), 371–373 (2008).
15. I. Fujieda and M. Ohta, "Angle-resolved photoluminescence spectrum of a uniform phosphor layer," *AIP Adv.* **7**, 105223 (2017).
16. R. Matsumura, Y. Tsutsumi, and I. Fujieda, "Concentric re-emission pattern from a planar waveguide with a thin uniform luminescent layer," *Appl. Opt.* **59**(6), 1703–1710 (2020).
17. I. Fujieda, Patent application JP-A-2002-14343 (in Japanese).
18. N. Koma et al., "Novel front-light system using fine-pitch patterned OLED," *J. Soc. Inf. Disp.* **17**(5), 473–479 (2009).
19. T. Large et al., "Far field imaging through liquid crystal displays for biometrics," in *SID Symp. Dig. Tech. Pap.*, Vol. 52, pp. 210–213 (2021).
20. S. Oka et al., "Ultra-narrow border display with a cover glass using liquid crystal displays with a polyimide substrate," *J. Soc. Inf. Disp.* **28**, 360–367 (2020).
21. D. Chowdhury et al., "Flexible glass substrate for OLED lighting application and efficient internal light extraction for OLED lighting devices," in *SID Symp. Dig. Tech. Pap.*, Vol. 51, pp. 93–95 (2020).
22. Y. Ukai et al., "Current status and future prospect of in-cell-polarizer technology," *J. Soc. Inf. Disp.* **13**(1), 17–24 (2005).
23. I. Fujieda, "Display device and driving method thereof," U.S. patent application 20030201960 (2003).
24. J.-H. Lee et al., "High ambient-contrast-ratio display using tandem reflective liquid crystal display and organic light-emitting device," *Opt. Express* **13**(23), 9431–9438 (2005).
25. Z. Luo, D. Xu, and S. Wu, "Emerging quantum-dots-enhanced LCDs," *J. Disp. Technol.* **10**(7), 526–539 (2014).
26. Z. Liu et al., "Micro-light-emitting diodes with quantum dots in display technology," *Light Sci. Appl.* **9**, 83 (2020).
27. A. Kim et al., "Review on colloidal quantum dots luminescent solar concentrators," *Chem. Select* **6**, 4948–4967 (2021).

**Tadamasa Anekawa** started his graduate studies at Ritsumeikan University in April 2022. He has been working on this project since December 2020.

**Mitsuhiro Shigeta** is an assistant professor at Ritsumeikan University. He received his PhD from Hiroshima University in 1983. He was with Sharp Corporation (1983 to 2015), Sakai Display Product Corporation (2015 to 2017), and the University of Shiga Prefecture (2017 to 2018) before joining Ritsumeikan University in 2018.

**Ichiro Fujieda** is a professor at Ritsumeikan University. He received his PhD from the University of California, Berkeley, in 1990. He was with Xerox Palo Alto Research Center (1990 to 1992) and NEC Corporation (1992 to 2003) before joining Ritsumeikan University in 2003.